THRUST MEASUREMENT FOR FLAPPING-FLIGHT COMPONENTS

Wolfgang Send*, Felix Scharstein**
ANIPROP GbR, Göttingen, Germany

Keywords: *Aerodynamics, Experimental facilities and techniques, Thrust measurement*

Abstract

A test stand named ANIPROP RL3 is introduced. The device allows the simultaneous recording of dynamic and kinematic quantities like thrust, lift and speed of components for biologically-inspired flight. The models are suspended from a boom and rotate around a hub on a circular path of about 6 m diameter. Thrust is described by an ordinary nonlinear differential equation for the components' velocity. The repeated solution of a system of nonlinear equations for various values of the velocity over the recorded period of time leads to a prediction of the thrust and all unknown coefficients.

1 Introduction

The thrust generated by the flapping-flight mechanism of a coupled bending/torsional motion is a complex matter for both the theoretical prediction and its measurement. Almost all current flapping-flight devices rest on a pure active plunge mechanism which – according to theoretical prediction – is said to be sufficient for generating thrust. A closer look at the location of this well known "suction force" accompanying the plunging motion reveals that it originates from the nose region of a profile within the first 2-3 % of the chord length. A less well known experimental work by Windsor [1] shows the decay of this force at angles of incidence larger than about 6 degrees (Fig. 2). Thus, the designers of flapping-flight devices are forced to admit a certain structural flexibility which results in a passive torsion of the wings. For this coupled bending/torsional motion the location of the suction force now stretches from the leading edge to the trailing edge as desirable. However, the aerodynamic efficiency

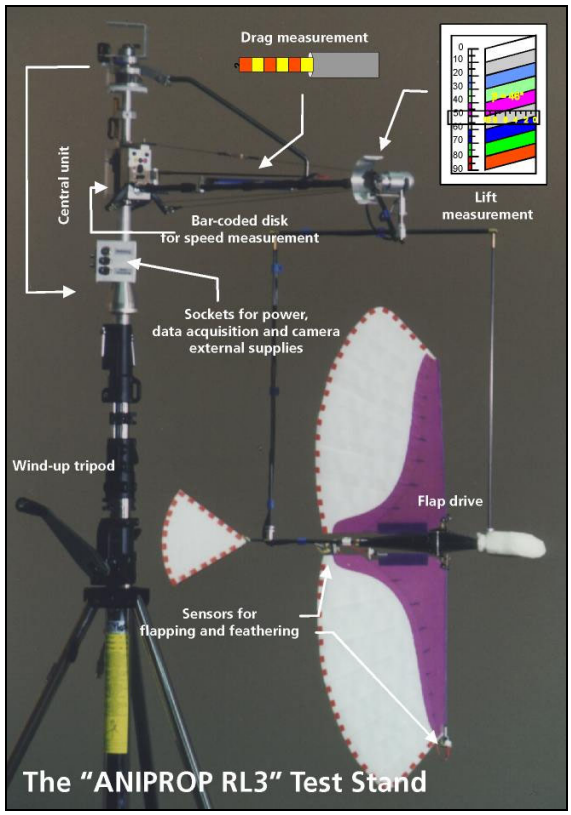

Fig. 1. The various parts of the device.

of active bending combined with passive torsion never exceeds 35-40 % and is very sensitive to the structural properties. It is the additional small amount of power driving an active torsion which raises the aerodynamic efficiency up to 80-90 %. The theoretical background may be found, among others, in earlier papers by Send

* Until October 2009, scientist at the German Aerospace Center (DLR), Institute of Aeroelasticity, Göttingen.
** Freelance precision mechanic, Berlin, Germany.

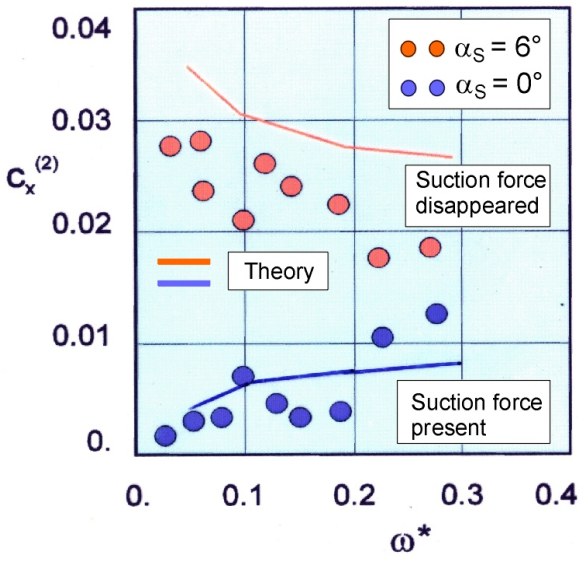

Fig. 2. Flat plate theory, unsteady mean drag coefficient $c_x^{(2)}$. Experimental data selected from Windsor's results. The negative suction force reduces the mean drag, if it is present. Theory includes (blue line) or ignores (red line) this second order term.

[2, 3, 4]. A basic introduction is summarized in chapter 3. These predictions were compared with experimental results gained from the RL3 using the simple artificial bird in Fig. 1 with a passive torsion [5].

The goal of the authors' current research is to identify the benefits from an active torsion predicted by all theoretical models ranging from classical potential theory to modern viscous flow CFD-solutions on an experimental basis using the test stand ANIPROP RL3.

2 Notation in the theoretical part

α_{0H}	Amplitude of $\dot{z}(t)/\dot{x}(t)$ for small angle
α_0	Amplitude pitch [rad]
α_S	Steady angle of incidence [rad]
h_0	Amplitude plunge [m]
c	Chord length [m]
S	Planform area of the wing
λ, λ_c	Amplitude ratio $= \dfrac{h_0}{\alpha_0 \cdot c/2}$, $\lambda_c = \lambda/2$
x, y, z	Space-fixed coordinates [m]
x^*, y^*, z^*	Body-fixed coordinate system [m]
f	Frequency [Hz] of periodic motion
ω	Circular frequency $= 2\pi f$ [1/s]
T	Period of cyclic motion $= 1/f$ [s]
t	Physical time [s]
u_0	Kinematic x-velocity [m/s]
X	Degree of freedom (DOF) {g, h, α}
ρ	Density of the fluid [kg/m³]
a_X	Dimensionless amplitude of DOF X $a_h = h_0/(c/2)$, $a_\alpha = \alpha_0$
$F_D(t)$	Drag force [N]
q_0	Dynamic pressure $= \frac{1}{2} \cdot \rho \cdot u_0^2$ [N/m²]
F_0	Force constant $= q_0 \cdot S$
$F_N^*(t)$	Force normal to the wing planform [N]
$F_L(t)$	Lift force [N]
$g(t)$	Motion, gliding: $g(t) = u_0 \cdot t$ [m]
$x(t)$	Motion, in x-direction $= -g(t)$ [m]
$z(t)$	Motion, in z-direction $= -h(t)$ [m]
$\alpha_H(t)$	Motion, apparent inflow angle [rad]
$\alpha_P(t)$	Motion, pitch $= \alpha_S + \alpha_0 \cos \omega t$ [rad]
$h(t)$	Motion, plunge $= h_0 \cos(\omega t + \kappa)$ [m]
κ	Phase shift of plunge versus pitch [rad]
x_L	Centre of steady pressure distribution
x_P	Pitch axis, absolute position
$P_X(t)$	Power at DOF X [W]
$c_{\Pi,X}(t)$	Power coefficient of DOF X $= P_X(t)/(F_0 \cdot u_0 \cdot \alpha_0^2)$
$< c_{\Pi,X} >$	Power coefficient averaged over T
η_{aero}	Aerodynamic (propulsive) efficiency
η_{mech}	Electro-mechanical efficiency
η_{total}	Total efficiency $\eta_{total} = \eta_{aero} \cdot \eta_{mech}$
ω^*, ω_c^*	Reduced frequency $\dfrac{\omega \cdot c/2}{u_0}$, $\omega_c^* = 2\omega^*$

The notation of the kinematics follows the notation in the classical papers [6,7,8]. For $t = 0$ the pitch angle is maximum positive. Without any phase shift ($\kappa = 0°$), the wing starts at the bottom in its lowest position. 3 shows a phase shift of $\kappa = 90°$, for which the highest pitch angle and the largest plunge velocity during upstroke coincide. The same phase shift leads to the interesting features in the centre of the graphs in Fig. 4.

For $P_X > 0$ power is consumed at DOF X and therefore is required for supplying the motion.

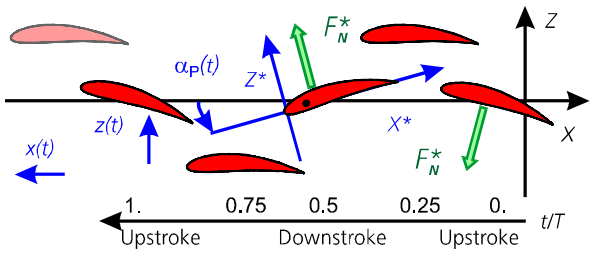

Fig. 3. 2D Kinematics and normal force F_N^*.

For $P_X < 0$ power is released at DOF X. Power is gained by the motion and has to be consumed for keeping the motion balanced.

3 The Focus of Interest in Brief

The translational motion $(x(t),z(t))$ of the 2D wing section (profile) in 3 leads to the angle $\alpha_H(t)$ of the slope

$$\tan\alpha_H(t) = \frac{\dot{z}(t)}{\dot{x}(t)} = \frac{h_0 \cdot \omega \cdot \sin(\omega t + \kappa)}{-u_0}. \qquad (1)$$

For small angles the tangent may be linearized by $\tan\alpha_H(t) \cong \alpha_H(t)$. With this assumption the amplitude of the angle of incidence due to the plunging motion can be expressed relatively to the pitch amplitude by the two coefficients λ and ω^*:

$$\frac{\alpha_{0H}}{\alpha_0} = \frac{h_0 \cdot \omega}{u_0 \cdot \alpha_0} = \lambda \cdot \omega^* = \lambda_c \cdot \omega_c^* \qquad (2)$$

The fluid's effect on the profile is like it would be rotated by the angle $\alpha_H(t)$. Moving in the fluid the profile experiences periodic normal forces due to the both motions pitch and plunge. While the normal force due to plunge does not rotate the profile geometrically, the pitch so does.

The normal force in the body-fixed coordinate system (3) can be estimated from the 2D lift formula for the inclined plate

$$F_N^*(t) \approx F_0 \cdot 2\pi\alpha(t), \qquad \alpha(t) = \alpha_P(t) + \alpha_H(t). \qquad (3)$$

The force in Eqn. (3) now is transformed into the reference system of the averaged translational motion, the direction of u_0.

$$\mathbf{F} = \begin{bmatrix} F_D \\ 0 \\ F_L \end{bmatrix} = \begin{bmatrix} F_N^* \cdot \sin\alpha_P \\ 0 \\ F_N^* \cdot \cos\alpha_P \end{bmatrix} \cong F_0 \cdot 2\pi \cdot \begin{bmatrix} \alpha_P^2 + \alpha_P \cdot \alpha_H \\ 0 \\ \alpha_P + \alpha_H \end{bmatrix} \qquad (4)$$

For small pitch angles $\sin\alpha \cong \alpha$ and $\cos\alpha \cong 1$ are applied, which gives the well known result that an unsteady harmonic motion produces a harmonically varying lift force and a drag force with the double period. As a consequence, the drag force averaged over one period of motion leads to a non-vanishing term, the mean thrust. In a more elaborate theory, the term in Eqn. (3) for the normal force is replaced by functions for the unsteady motion in which the shedding vortices lead to delayed or advancing reactions of the forces relative to the kinematic motion. The corresponding powers are given by *force × velocity*

$$P_{trans} = \mathbf{F} \cdot \mathbf{v}_{kin}, \quad \mathbf{v}_{kin} = -[\dot{x},0,\dot{z}] \qquad (5)$$

and *moment × angular velocity*

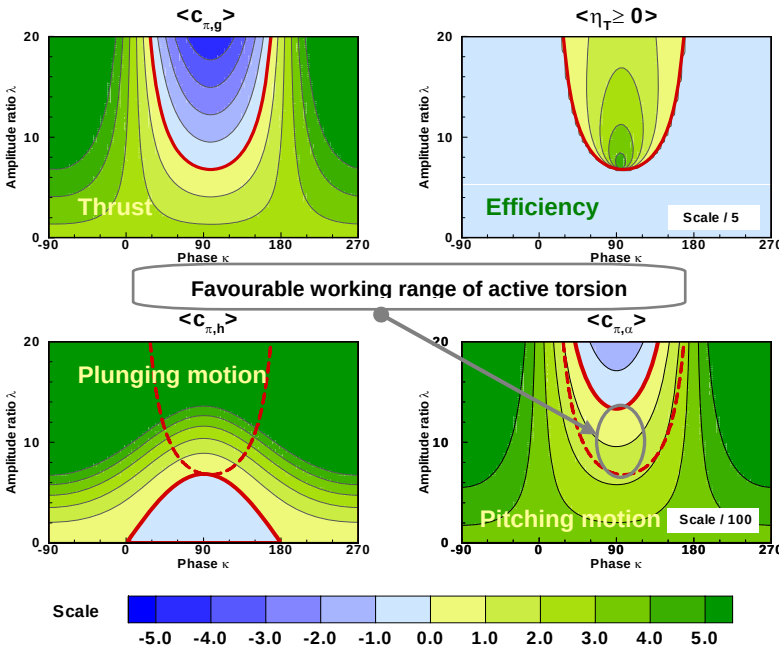

Fig. 4. Mechanism of propulsion, 2D thin plate.
$\omega^* = 0.15,\ x_P/c = 0.25.$

$$P_{rot} = M_P(t) \cdot \left[-\dot{\alpha}_P(t)\right],\ M_P(t) = F_N^*(t) \cdot \left(x_P - x_L\right). \quad (6)$$

The force **F** in the preceding equations is the reaction force of the fluid on the moving body. Thus, the velocity in the formulas has to be the kinematic motion of the fluid relative to the body, which is the negative value of the body's velocity in the fluid. The fluid is at rest.

If the centre of the pressure distribution x_L is close to or even coincides with the centre of rotation x_P, the power due to rotation is negligible in the quasi-steady case.

The basic mechanism of thrust generation is understood after evaluating Eqn. (5). The translational power is split into the contributions from the DOFs *g* and *h:*

$$P_{trans} = P_g + P_h = -F_D \cdot \dot{x} - F_L \cdot \dot{z} \quad (7)$$

A straightforward calculation leads to $P_g(t)$ and $P_h(t)$. From the mean value during one cycle of motion

$$< P_X > = \tfrac{1}{T} \int_0^T P_X(t) \cdot dt \quad (8)$$

the power coefficients are computed, given by

$$< c_{\Pi,X} > = \frac{< P_X >}{F_0 \cdot u_0 \cdot \alpha_0^2} \cdot \quad (9)$$

In the simplified approach, results for the translational motions read

$$< c_{\Pi,g} > = -\pi \cdot \left[\omega^* \lambda \cdot \sin\kappa - 1\right], \quad (10)$$

$$< c_{\Pi,h} > = +\pi \omega^* \lambda \cdot \left[\omega^* \lambda - \sin\kappa\right]. \quad (11)$$

For the favourable case $\kappa = 90°$ thrust is gained for $\omega^* \lambda > 1$. From the definition in Eqn. (2) propulsion is effected by a large plunging motion for which the amplitude of the apparent inflow angle $\alpha_H(t)$ is larger than the amplitude of the geometric pitch angle $\alpha_P(t)$. The propulsive or aerodynamic efficiency η_T is given by

$$\eta_T = \frac{- < c_{\Pi,g} >}{< c_{\Pi,h} > + < c_{\Pi,\alpha} >}, \quad < c_{\Pi,g} > < 0 \cdot \quad (12)$$

4 Efficiencies

The overall or total efficiency η_{total} of a flapping-flight component is given by the thrust power gained from the engine, the output, compared to the energy input. The thrust power balances the drag and the weight of the device. The efficiency of this process is composed of at least two different constituents, the electro-mechanical efficiency η_{mech} and the propulsive or aerodynamic efficiency η_{aero}, i.e. η_T in Eqn. (12).

$$\eta_{total} = \eta_{aero} \cdot \eta_{mech} \quad (13)$$

The aerodynamic efficiency is a theoretical prediction, which needs to be checked in an appropriate experiment. Eqn. (12) is the predicted efficiency of a 2D pitching and plunging thin plate. The result for the well known analytical solution in incompressible flow is shown in Fig. 4. The four graphs in the figure display the basic features of animal flight. Whereas the power coefficients in Eqns. (10) and (11) solely are based on the kinematic relations, the physical model behind these for graphs also includes the unsteady wake field of the vortices travelling downstream. Their influence causes the phase shifts between the motion and the resulting forces and moments. In particular, the power coefficient of the pitching motion reveals a fundamental property of animal flight, over and above that, of the mechanism of coupled bending and torsional motion in general. The motion becomes extremely efficient for an active torsion and then converts almost all input power into thrust. Active torsion takes place in the circled area in Fig. 4. The graph shows, that the torsion acts like a catalyst for the mechanism. It requires hardly any power, but needs to be present.

Historic remark. In 1929, at the time Alexander Lippisch made his famous experiments with flapping-flight airplanes, the theoretical background of aerodynamic efficiency predicting the importance of active torsion was not yet developed. The very first paper on unsteady experiments in a wind tunnel had appeared a couple of years ago. The experiments had been carried out by Katzmayr [9] in Vienna. Lippisch refers to Katzmayr's work in

the paper in which he describes years later his experiments with flapping-flight drives [10]:

.. After testing the ship a few times in gliding, Hans Werner [Krause] tried the first flapping-wing flights. The result was quite disappointing, since we could not see any improvement of the glide angle. At least the effect was so small that the measured Katzmayr effect did not show up, and the twisting of the wings, even with this light construction, did not occur. At first we did not know what to do next.

To find out how to improve things I made some tests with a model wing, and ***I clearly observed that a stiff wing in flapping motion did not produce any forward thrust.***[1] *I then remembered that some of the stories from early years told about a flexible trailing edge. I therefore enlarged the outer portion of the wing by the addition of a flexible (single bamboo sticks) Zanonia-like rear surface as shown in the sketch. The piece was not very large but what a difference in propulsive action was caused by this change! ...*

5 Concept of the Test Stand ANIPROP RL3

The rotating boom of the test stand consists of two rods, which are connected to each other by a hinge named *joint-head* G_k with one degree of freedom. The *inner boom* R_i remains horizontal during the motion, the *outer boom* R_a is in a vertical position for the boom at rest. The angle enclosed by the outer boom and the horizontal is denoted as *centrifugal angle* β. Fig. 5 shows the side view of the geometric relations.

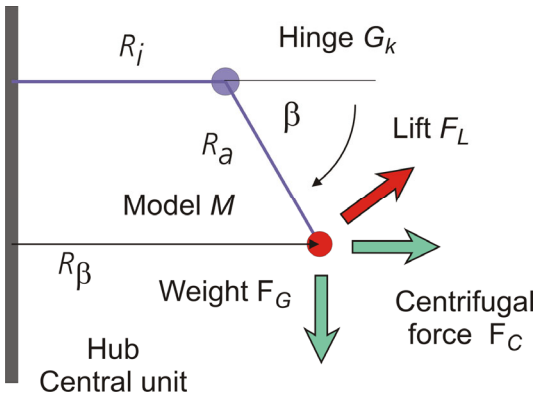

Fig. 5. Geometry of the boom - side view.

The distance R_β of the centre of gravity of the model M investigated to the axis of rotation is given by

$$R_\beta = R_i + R_a \cdot \cos\beta \qquad (14)$$

The model experiences three forces, the gravitational force F_G, the centrifugal force F_C, and the lift force F_L. The decomposition of the three forces into a horizontal component and a vertical component immediately leads to a formula for the lift force

$$F_L = M \cdot \cos\beta \cdot \left[g - \omega^2 \cdot R_\beta \cdot \tan\beta\right] \qquad (15)$$

The inner part of the square bracket is the relation for the circular motion of a mass on a rotating string. ω is the circular frequency of the rotation and g the gravitational acceleration. The expression vanishes for a point mass which experiences no further force. In the presence of a lift force the angle β either decreases for positive lift or increases for negative lift.

- Thus, the measurement of the lift force on the model M is carried out by determining the centrifugal angle β and the angular velocity ω.

For a non-uniform motion the angular velocity is given by the time derivative of $\varphi(t)$.

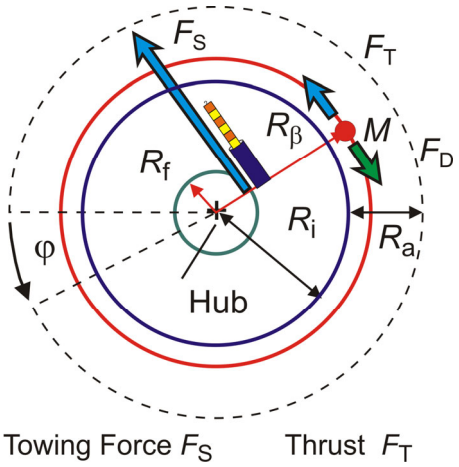

Fig. 6. Geometry of the boom - top view.

The boom is towed by a lever which is driven by an electric motor. The point of origin of the towing force F_S is distant to the axis of rotation

[1] Phrase highlighted by the author. Thrust by a pure plunging motion still is a very controversial issue among aerodynamicists.

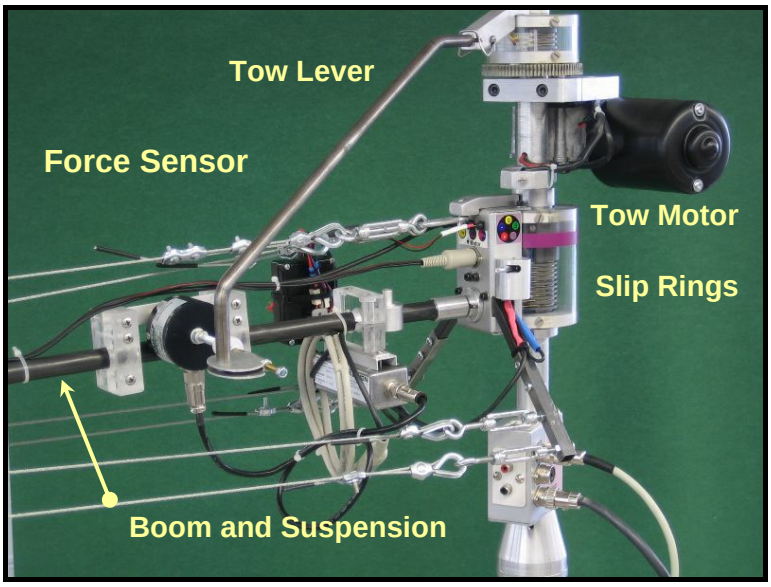

Fig. 7. Central unit of the RL3. The lever tows the boom via a force sensor which is connected to an amplifier. Power supply and signals are transmitted using slip rings. The electric motor in the upper right corner works as gearwheel drive. The height is about 0.6 m.

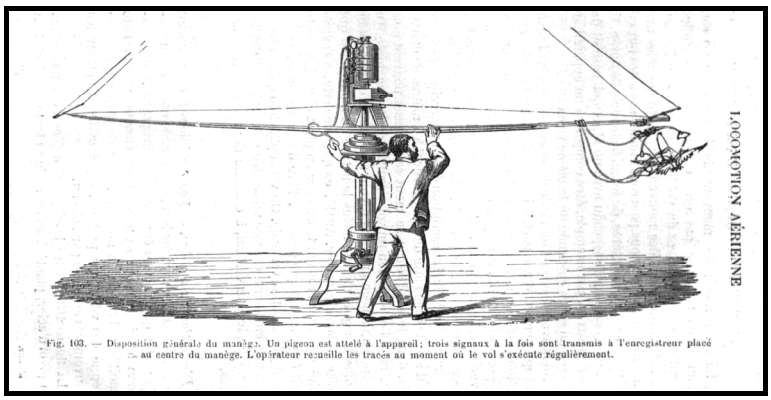

Fig. 8. Apparatus designed by Étienne-Jules Marey (1830-1904). Investigation of life birds equipped with pressure sensors [11].

by the length R_f (the moment arm). The spring scale symbolizes the force measurement, and is located between the lever and the boom. For the purpose of demonstrations, the measurement indeed is carried out using a spring scale. The elongation of the scale is available as an electric signal. For more accurate measurements, the spring scale is replaced by a force sensor.

The total drag of the boom including the aerodynamic drag of the boom and the friction of the bearings is given by

$$F_D = (R_f / R_\beta) \cdot F_S \qquad (16)$$

It is worth mentioning that this concept is not entirely new. Otto Lilienthal designed a test stand for the measurement of lifting surfaces [12]. Even closer to the RL3's concept is the apparatus depicted in Fig. 8. It was developed by the French scientist Étienne-J. Marey. Pressure sensors allowed the recording of the birds' kinematics. The simple artificial bird in Fig. 1 is equipped with two sensors for the two degrees of freedom pitch and plunge.

6 Data acquisition

The data acquisition system belonging to the RL3 is laid out for the recording of ten signals.

1	Towing force
2	Centrifugal angle
3	Voltage tow motor
4	Voltage flapping device
5	Current tow motor
6	Current flapping device
7	Pitch angle (feathering)
8	Plunge angle (flapping)
9	Speed marks
10	Position marks

All signals including the marks for speed and position are analogue signals. An A/D card converts the signals for digital processing in a computer. Speed marks are sent 180 times per revolution, i.e. each 2 degrees, the position mark is sent once per revolution. The purpose of the position mark is to relate anomalies in the data to the position of the model in the test hall.

A large number of physical quantities can be derived from the input signals. The basic quantities are

- the velocity u_0 of the moving model,
- the total drag force F_D in Eqn. (16),
- the lift force F_L according to Eqn. (15),
- the electric power P_F consumed by the flapping-flight component.

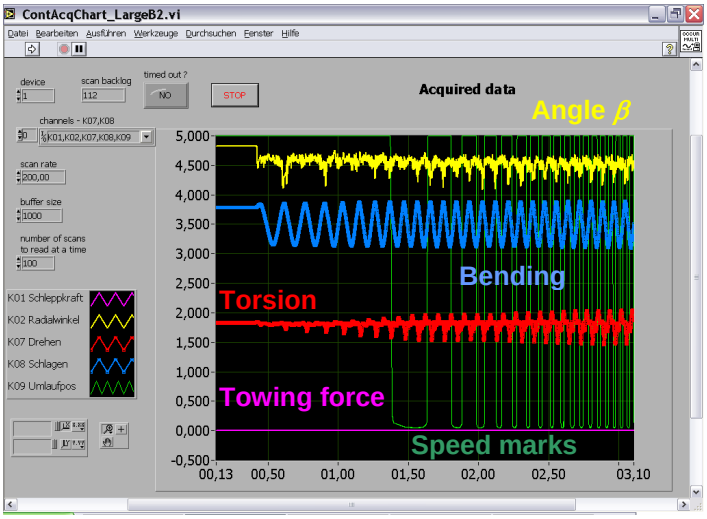

Fig. 9. Start of the artificial bird in free mode. Passive torsion is forced with beginning motion.

7 Operating the test stand RL3

Thrust measurements with the RL3 may be carried out in two different modes. In the *free mode* the tow lever is removed. The model starts from a position at rest. Fig. 9 shows the increase of passive torsion after the start and a raising amplitude with increasing speed. In Fig. 4 the corresponding operating range is the blue coloured area for pitch where the motion consumes power (lower right graph).

The *tethered mode* uses the tow lever which is symbolized by a spring scale in Fig. 6. The boom with the model is driven by the electric motor installed on the central unit. For a given speed, the spring scale, the force sensor respectively, indicates the drag. If the flap mechanism is turned on, the drag is reduced by the amount of thrust generated. Fig. 10 shows a typical measurement. At the beginning, the flapping mechanism is turned off. The towing force (blue line) coincides with the steady drag (green line). Then the mechanism is turned on. F_S decreases by the amount of thrust which now is generated. During the measurement the thrust gradually is decreased until the uniform steady motion is reached again.

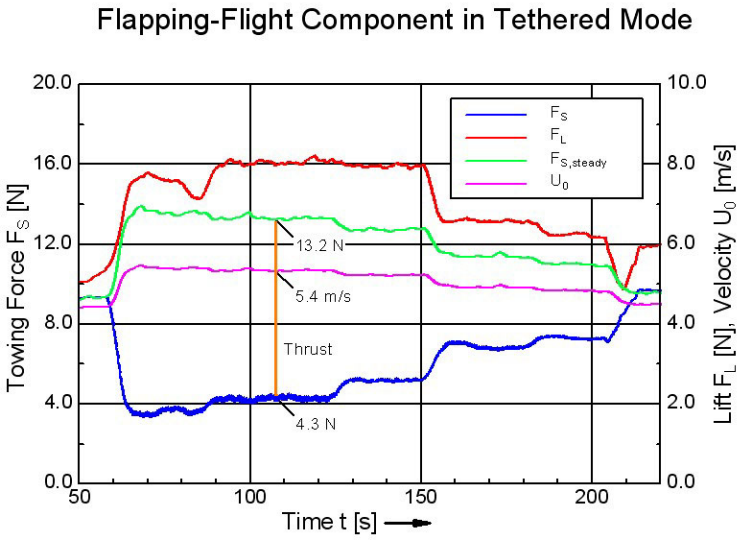

Fig. 10. Typical thrust measurement in tethered mode.

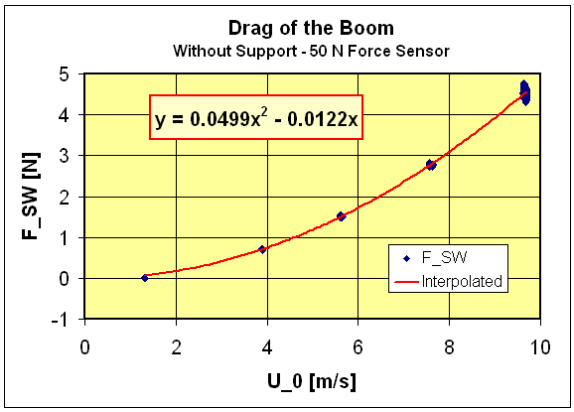

Fig. 11. Drag curve of the boom.

The difference in lift at the beginning and at the end is caused by a slightly different position of the wings, which simply results from manually turning off the power. The model possesses no “lock-in” mechanism, which stops the flapping wings at a preset position for steady flight.

The data processing implies several steps which complicate the evaluation. They are not discussed here in detail. For example, a closer look at the towing force in Fig. 10 shows a higher value at the end than at the beginning. This is caused be the increased lift. The difference is responsible for a slightly higher induced drag. Its absolute amount is scaled by the ratio in Eqn. (16).

The total drag immediately leads to the total power which is consumed by the towed model. The model's aerodynamic drag is obtained by subtracting the drag of the boom from the total drag. Fig. 7 shows a typical curve for the boom's drag. The caption in the figure tells that the drag of the support for the model is not yet included, which gives an additional small contribution.

8 Electromechanical efficiency

The total efficiency is determined by the ratio of gained thrust power to electric power consumed by the model. This ratio is not yet the predicted aerodynamic efficiency in Eqn. (12), which cannot be measured directly. The evaluation of the aerodynamic efficiency requires the determination of the electromechanical efficiency of the respective flapping-flight component.

This is step #1 for verifying the high aerodynamic efficiency of the active torsion. The device in Fig. 12 determines the electromechanical efficiency. The upstroke and downstroke of the wings is transferred to two levers (one of them is sketched in red). They are fixed on the horizontal axis of a device which frequently is named *Prony brake*. The more or less tightened brake shoe forms the end of a moment arm which is held by a force sensor. The flapping motion causes a cyclic motion of the horizontal axis, which is measured by a rotary inductive position sensor indicating the angular velocity. Force and lever form a moment of force, which - multiplied by the angular velocity - results in the available mechanical power.

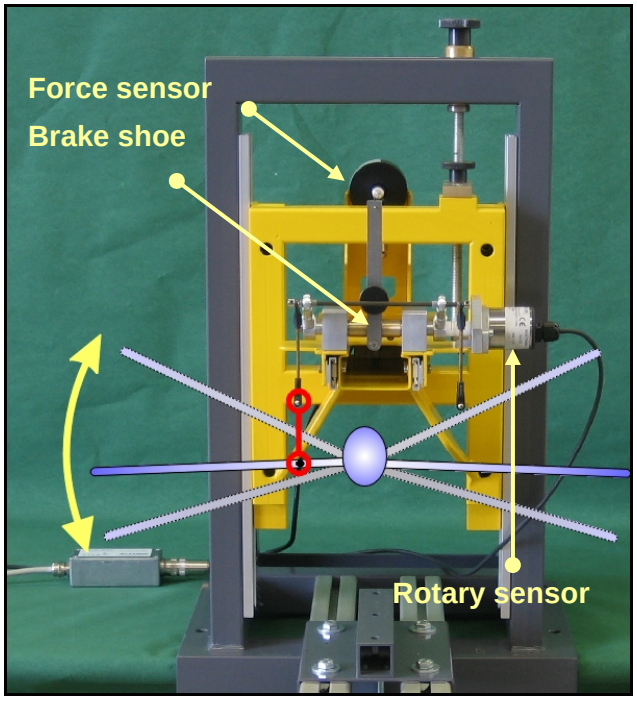

Fig. 12. *Prony brake* for the measurement of electromechanical efficiency of flapping-flight components - sketch of the wing motion.

Step 1: $\eta_{mech} = \frac{availabe\ \ mechanical\ \ power}{supplied\ \ electric\ \ power}$
Step 2: $\eta_{total} = \frac{gained\ \ thrust\ \ power}{supplied\ \ electric\ \ power}$
Step 3: $\eta_{aero} = \frac{gained\ \ thrust\ \ power}{supplied\ \ mechanical\ \ power}$

The experiment with the towed model provides the data which are shown in Fig. 10. This is step #2 in the case of the *tethered mode*. The next step #3 gives the result for the aerodynamic efficiency:

$$\eta_{aero} = \frac{\eta_{total}}{\eta_{mech}} \qquad (17)$$

The verification of the theoretical predictions critically depends on the careful measurement of the electromechanical efficiency of the flapping-flight model.

9 Direct thrust measurement

While the determination of thrust in tethered mode is easily accomplished, its evaluation in free mode requires more effort. The measurement done in free mode is named *direct thrust measurement.* From the physical point of view, this is the result which is comparable to the thrust data given for a customary airplane engine, except that the typical values are smaller by several magnitudes. The flapping-flight model is mounted in a support frame and suspended from the boom like shown in Fig. 1.

In a preliminary step the moment of inertia J_F of the model including the boom and the support is determined. This is done by accelerating the joint-head by a falling mass. The configuration is displayed in Fig. 13. The joint-head G_k is connected via a thin nylon

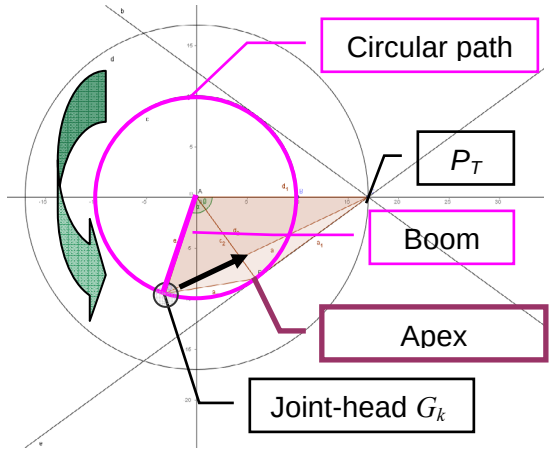

Fig. 13. Geometry of the direct thrust measurement with the outer boom kept vertically. Test stand seen from above.

thread to a guide pulley at the fixed point P_T and from there to a mass m_T of known weight which hangs at the end of the thread. Then, the joint-head G_k is released and the boom with all parts is accelerated. Close to the apex of the circular motion, where the direction of traction of the nylon thread is nearly perpendicular to the boom, the motion may be treated as being linear instead being circular. With this assumption, the equations

$$m_T \cdot g = M_F \cdot a_F \,,\; J_F = M_F \cdot R_i^2 \qquad (18)$$

give the unknown moment of inertia J_F. The constant g is the gravitational acceleration and the acceleration a_F is determined from time derivative of the velocity measurement of the rotating boom. The following table gives an impression of the accuracy which might be achieved.

Weight m_T, Record #	J_F [kg m²]
50 g 01	1.1386
50 g 02	1.2503
50 g 03	1.1689
100g 04	1.0713
100g 05	1.1809
100g 06	1.1027
Average	**1.1521**
M_F	**0.319 kg**

Tab. 1. Moment of inertia J_F and equivalent point mass M_F for a typical configuration.

Once the moment of inertia is determined, the ordinary differential equation for the

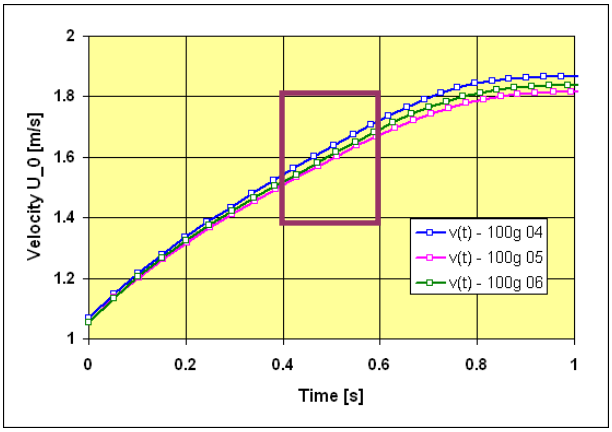

Fig. 14. Set of velocity data for determining the moment of inertia. The boxed area near the apex is evaluated (acceleration $a_F \sim 0.8$ m/s²).

unknown thrust F_T is set up. Again, the circular motion is treated as being a linear motion. A further assumption is a constant thrust. The following equation includes a friction term k proportional to velocity and the aerodynamic drag coefficient r proportional to the square of velocity

$$M_F \cdot \dot{u}(t) + r \cdot u^2(t) + k \cdot u(t) = F_T \qquad (19)$$

The equation for the velocity $u(t)$ is solved by

$$u(t) = -u_k + u_0 \cdot \tanh\left[(t - t_0)/t_c\right] \qquad (20)$$

with the constants given by

$$u_k = \frac{k}{2r},\; r \cdot \left(u_0^2 - u_k^2\right) = F_T \,,\; t_c = \frac{M_F}{r \cdot u_0} \qquad (21)$$

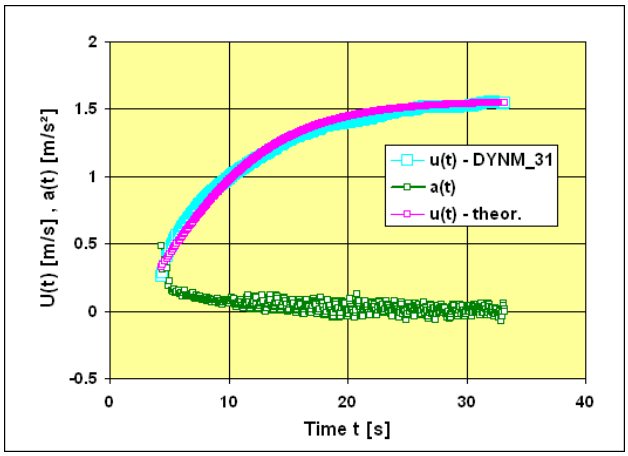

Fig. 15. Velocity and acceleration over time t, measurement and theoretical reconstruction.

The unknown three physical constants r, k and F_T are determined by the following procedure. Eqn. (21) implies the four unknown constants u_k, u_0, t_0 and t_c. The set of N measured data

$$\{n, t_n, u_n(t_n); n = 1, \ldots, N\} \qquad (22)$$

is divided into four quarters. Then, any four pairs of data $\{i, t_i, u_i(t_i); i = 1,2,3,4\}$ are selected close to the beginning of each quarter. The four selections form a set of nonlinear equations with $F_i = 0$ for the four constants u_k, u_0, t_0 and t_c.:

```
F1(u0,tc,t0,uk) = -u1-uk+u0*tanh ((t1-t0)/tc)
F2(u0,tc,t0,uk) = -u2-uk+u0*tanh ((t2-t0)/tc)
F3(u0,tc,t0,uk) = -u3-uk+u0*tanh ((t3-t0)/tc)
F4(u0,tc,t0,uk) = -u4-uk+u0*tanh ((t4-t0)/tc)
```

The four equations are solved using the subroutine DNEQNF in the IMSL [13] for systems of nonlinear equations. The solution algorithm requires an initial guess. It is suggested to solve the system initially for $k = 0$, because k is a small quantity. The equations then read:

```
F1i(u0,tc,t0) = -u1+u0*tanh ((t1-t0)/tc)
F2i(u0,tc,t0) = -u2+u0*tanh ((t2-t0)/tc)
F3i(u0,tc,t0) = -u3+u0*tanh ((t3-t0)/tc)
```

A sweep over the four quarters of the time interval with a successive solution for several sets of every time four pairs leads to an averaged solution for r, k and F_T with the option of computing error estimates.

10 Outlook

At present, the search for the high efficiency of the active torsion is in the state of a thorough validation of the results for various flapping-flight components and artificial birds.

The procedure described in this paper reflects the current state of the art of the authors' approach to a better understanding of animal-flight performance.

References

[1] Windsor R I. Measurement of Aerodynamic Forces on an Oscillating Airfoil. *US Army Aviation Materiel Laboratories Fort Eustis VA,* USAAVLABS Technical Report 69-98, 1970.

[2] Send W. The Mean Power of Forces and Moments in Unsteady Aerodynamics, *Zeitschrift für angewandte Mathematik und Mechanik (ZAMM)* **72**, pp 113-132, 1992.

[3] Send W. Der Traum vom Fliegen, *Naturwissenschaftliche Rundschau* **56**, Heft 2, pp 65-73, 2003.

[4] Send W. Flapping-Wing Thrust in Compressible Flow, ICAS 2006-3.10.4, 25th ICAS Congress Hamburg, 3-6 Sep 2006.

[5] Send W, Scharstein F. Artificial Bird in Tethered Flight - Demonstration and Aerodynamics, *Biona Report 13 - Motion Systems*, Gustav Fischer Verlag, Stuttgart 1998, 195-196.

[6] Küssner H G. Zusammenfassender Bericht über den instationären Auftrieb von Flügeln, *Luftfahrtforschung* **13**, pp 410-424, 1936.

[7] Theordorsen Th. General Theory of Aerodynamic Instability and the Mechanism of Flutter, N.A.C.A. Report No. 496, 1935.

[8] Garrick I E. Propulsion of a Flapping and Oscillating Airfoil, N.A.C.A. Report No. 567, 1936.

[9] Katzmayr R. Über das Verhalten der Flügelflächen bei periodischen Änderungen der Geschwindigkeitsrichtung, Z. f. Flugtechnik und Motorluftschiffahrt 6 (1922), 80-82, Schluß: 7 (1922), 95-101.

[10] Lippisch A M. Man Powered Flight in 1929, *Journal of the Royal Aeronautical Society*, Vol. 64 (July 1960), 395-398

[11] Marey E J. La Machine Animale, Paris 1891, Cinquième Édition, Éditeur F. Alcan.

[12] Lilienthal O. Der Vogelflug als Grundlage der Fliegekunst, R. Gaertners Verlagsbuchhandlung, Berlin 1889

[13] International Mathematical and Statistical Library (IMSL). Version 1, Houston, Texas 1989. www.vni.com/products/imsl/fortran/overview.php

Copyright Statement